TECHNICAL ARTICLE

Study of Tribological Properties of Bulk Nanostructured Aluminum and Copper Samples Applicable in Automotive Bearing Application

Mehdi Eskandarzade, Tahereh Masalehdan, Abolfazl Tutunchi, Karim Osouli-Bostanabad [iD], Robin Hildyard, Stephen Rickie Bewsher, and Mahdi Mohammadpour

Using lightweight systems and friction reduction approaches are two main contributors towards modern and efficient powertrains in the automotive industry. New materials and processes are required to achieve the demanding and ever-increasing performance requirement of automotive systems. Nanostructure induced by severe plastic deformation methods involves bimodal microstructures and hence, shows exceptional mechanical characteristics which can be exploited for automotive application. Through this study, samples were prepared using pure copper, aluminum alloy (series 7000) and were processed to attain bulk nanostructured samples using a Single Step High Pressure Torsion technique with appropriate dimensions applicable as the rolling elements of automotive bearings. The induced nanostructures resulted micro hardness and frictional characteristics of the bulk samples were assessed using transmission electron (TEM) and atomic force (AFM) microscopies as well as microhardness evaluations. The results revealed that a fully refined nanostructured samples were achieved with 90% increase in the hardness at the outer diameter of the sample. The AFM measurements indicated that the friction coefficient of nanostructured copper and aluminum samples were $\sim$ 25 and $\sim$ 45% less than that of both the unprocessed samples, respectively. Characteristics of treated samples suggest that these processes can be potentially used in demanding conditions of rolling element bearings with reduced weight and frictional losses.

List of Symbols	
A	Real contact area
E	Modulus of Elasticity
F_n	Normal load
r_p	Average radii of curvature of asperity tips
d	Extent of deformation
F_a	Adhesive friction
H	Hardness
R_q	Root-mean-square roughness
E^*	Equivalent reduced elastic modulus
F_d	Deformation friction
K	A constant
S_q	Root-mean-square roughness of the scanned area

Greek Symbols	
ζ	Coefficient of Friction
τ_s	Shear strength of the softer counter face material
σ	Combined root-mean-square of surface asperity heights
υ	Poisson's ratio

Abbreviations	
AFM	Atomic Force Microscopy
NS	Nanostructured
TEM	Transmission Electron Microscopy
COF	Coefficient of friction
SIHPT	Single Step High Pressure Torsion
EDE	Electric Discharge Erosion
LFM	Lateral force microscopy
SPD	Severe Plastic Deformation
FIB	Focused ion beam

1. Introduction

An increasing demand exists for development of tribologically high performance, lightweight materials especially in the automotive industry. The lightweight and efficient material is particularly important for rolling element bearings of high speed electric powertrains which tend to operate at tens of thousands revolutions per minute in order to increase the

Mehdi Eskandarzade, Department of Mechanical Engineering, University of Mohaghegh Ardabili, Ardabil, Iran; **Tahereh Masalehdan** and **Abolfazl Tutunchi**, Department of Materials Engineering, Institute of Mechanical Engineering, University of Tabriz, Tabriz 51666-16444, Iran; **Karim Osouli-Bostanabad**, Institute of Biomedical and Biomolecular Sciences, School of Pharmacy and Biomedical Sciences, University of Portsmouth, White Swan Road, Portsmouth PO1 2DT, UK; and School of Pharmacy and Biomedical Sciences, Robertson Wing, University of Strathclyde, 161, Cathedral Street, Glasgow G4 0RE, Scotland, UK; **Robin Hildyard, Stephen Rickie Bewsher,** and **Mahdi Mohammadpour**, Wolfson School of Mechanical, Electrical and Manufacturing Engineering, Loughborough University, Loughborough, UK. Contact e-mails: m.eskandarzade@uma.ac.ir, karim.osouli-bostanabad@port.ac.uk, and karim.osouli-bostanabad@strath.ac.uk.

efficiency of the overall system (Ref 1). At these speeds, the dynamics of rolling element (rollers) which can normally be neglected at moderate or low speeds, become significant. Hence, there is a great potential for any process which can enhance the performance and applicability of materials such as Severe Plastic Deformation (SPD) processed copper or lighter aluminum for bearing applications.

It is now well-established that microstructure refinement in bulk metals and nano-structuring these metals can significantly improve their mechanical properties (Ref 2). For instance, more than a two-fold enhancement in tensile strength of pure and alloyed metals is reported through microstructural grain refinement (Ref 3). Recently, SPD has emerged as a promising technique to produce nanostructured (NS) components. Although most scientific investigations have focused on various characteristics of bulk NS samples, including tensile strength (Ref 4), thermal properties (Ref 5), magnetic behavior (Ref 6), energy conversion and storage (Ref 7), corrosion (Ref 8), super-plasticity (Ref 9) and low temperature super-plastic properties (Ref 10), but there have been less detailed studies on the tribological performance of NS samples. While a few assessments addressing the frictional properties of bulk NS samples, enormous amounts of reported works deal with frictional properties of NS coatings (Ref 11-14). Prasad et al., (Ref 15) concluded that the production of stable NS films beneath sliding surfaces at high contact pressures is responsible for the drastic changes in the coefficient of friction (COF) that increases with the sliding distance augmentation. Henry et al. (Ref 16) showed that the friction reduction in a nanocrystalline Ni-Fe alloy depends on the sliding speeds. They revealed that nano-structuring led to reduction of friction particularly at low sliding speeds. Various findings on the wear and frictional behavior of SPD-treated materials were summarized by Gao et al. (Ref 17). They argue that the COF seems to depend on many parameters such as the type of material, the method of nano-structuring and lubrication conditions. The effect of lattice defects on frictional properties of NS samples using pin on disc has been reported by Tonotsuka et al. (Ref 18). They reported that in lubrication regime NS samples show higher friction than the undeformed samples. Manjunath et al., (Ref 19) reported that the nano-structuring of Al-10Zn-2Mg alloy helps to improve the tribological properties of the samples. In addition, Su et al. (Ref 20) reported superior frictional properties of aluminum alloys after subject to SPD. As mentioned above, novel lightweight materials with lower friction in the moving components with the capability of preserving a required level of mechanical properties is one of the potential methods to achieve more efficient systems in the automotive industry. The lightweight characteristic is particularly important from a dynamics point of view for ultra-high speed bearings (Ref 1).

It should be noted that friction, as a result of surface interaction always comes with wear. Although the wear performance of proposed material here should be investigated and established as a future research subject, it is well established that the hardness and hence the wear will improve by SPD process (Ref 21).

In bearing application, the regime of lubrication depends on working conditions and lubricant properties such as viscosity, density and other rheological characteristics. In most cases, the dominant regime is a mixed regime of lubrication (a combination of fluid film and boundary; i.e., direct interaction of surface roughness). SPD, by its nature, affects the surface and boundary interaction part of the friction rather than the fluid film formation. Hence, in this paper with a focus on effect of SPD as a process on lubrication of bearings, only the boundary regime is investigated.

To understand the frictional characteristics of a NS material under the boundary regime of lubrication, it is important to investigate the different friction generating mechanisms. One of main friction sources is the shear strength of the surface asperities on the softer of the counter face (τ_s), which has a relation with real contact area (A) as $F_a = A\tau_s$. The real contact area is the determining parameter in specifying adhesive friction (F_a). By assuming plastic deformation at asperities, the real contact area can be estimated by simply dividing normal carried load (F_n) to softer material hardness (H). However, in the case of elastic deformation, the real contact area can be obtained via Eq 1 (Ref 22):

$$A \approx 3.2 \frac{F_n}{E^*} \sqrt{\frac{r_p}{\sigma}} \qquad (\text{Eq 1})$$

where r_p is the average radius of curvature of asperity tips and σ is the root-mean-square of surface asperity heights. E^* is the reduced Young's modulus of elasticity of the contacting solid pairs, defined as: $\frac{1}{E^*} = \frac{1-v_1^2}{E_1} + \frac{1-v_2^2}{E_2}$. As the previously mentioned equations show, F_a is inversely proportional to either material hardness or the contact reduced modulus of elasticity. Both of these quantities increase with grain size reduction (Ref 23). For a NS material, the hardness increases by reducing its grain size, which leads to a reduction in friction.

Another friction mechanism is through asperity ploughing, caused by the deformation of the softer counter face asperities by those on the harder counter face surface. If the deformation occurs in the plastic region, due to the plastic deformation (F_d), friction can be estimated by knowing the depth of the deformation (d) as $F_d = \pi d^2 H$ (Ref 24). If asperities undergo elastic deformation, a similar expression can be used in order to estimate the generated friction (Eq 2) (Ref 25):

$$F_d = \pi d^2 E^* \sqrt{\frac{\sigma}{r_p}} \qquad (\text{Eq 2})$$

Unlike the adhesive friction, the ploughing friction is proportional to the hardness and the reduced elastic modulus. Contradictory characteristics of friction in NS materials make it a complex phenomenon. Farhat et al. (Ref 26) has measured the COF between an NS aluminum film deposited on an aluminum disc and a steel miniature pin. They reported the friction coefficient reduction of more than 55% in NS samples compared to that of a coarse grain structure aluminum disk under similar test conditions. The thickness of NS aluminum film and the grain size in their experiment were approximately 10 μm and 15-100 nm, respectively. They also found that the hardness of the substrate disc affected the mechanism of friction generation, showing the different frictional behavior of the NS film in comparison with the bulk NS component. Peng et al. (Ref 27) has studied the effect of grain size on the generated friction in adhesion-dominated and ploughing-dominated regimes of friction. They found that with an increasing grain size, the COF enhances with adhesion and decreases with ploughing. A study based on large-scale molecular dynamics simulation by Beckmann et al. (Ref 28) showed that using NS

patterns on the sliding surfaces can improve wear resistance. The results of a similar study using molecular dynamics also revealed the importance of grain size on the friction which can be sensitive to contact dimensions (Ref 29).

Introducing a bimodal grain size distribution has been demonstrated an efficient strategy for fabricating high-strength and ductile metallic materials, where fine grains provide strength, while coarse grains enable strain hardening and hence decent ductility (Ref 30). In this study, a recently developed Single Step High Pressure Torsion (SIHPT) process (Ref 21), was used to produce NS samples of bulk pure copper and aluminum alloy (series 7000) as candidate materials for efficient roller bearing designs. In modern powertrains, in particular electrified systems, the range of speed has significantly increased in comparison with traditional internal combustion engines. Under these high speeds, and with the presence of electric field due to electromagnetic effects in the system, two new challenges arise: (1) significant dynamic behavior of rollers and balls in rolling element bearings (Ref 31), leading to noise and durability problems and (2) a new failure mode of Electric Discharge Erosion (EDE) in contacts (Ref 32). Aluminum as one of the selected candidates in this study provides significantly lower density, being a great choice to tackle rollers and balls high inertial dynamics. Copper as the second choice provide new ranges of electric conductivity as alternative to steel rollers and balls, which will allow powertrain developers to potentially utilize them to manage EDE at a system level. It should be noted that the main aim of this research is not to provide a design recommendation, but rather providing more material options to developers to tackle abovementioned issues. Thereby, effects of nano-structuring on mechanical and frictional characteristics of the processed samples were investigated. The process was designed to prepare samples potentially applicable as rolling elements of bearings at automotive applications, size wise. The nano structure of the processed samples was characterized using transmission electron microscopy (TEM) to attain the grain structure refinement level of the samples. The frictional characteristics of the sample were evaluated conducting an atomic force microscope (AFM). The presented research on the effect of SPD technique on pure copper and commercial aluminum alloy for obtaining superior hard surface and frictional characteristics appropriate for automotive applications has not been reported hitherto. Therefore, the goal of this study was to investigate and compare the unprocessed and processed samples using copper and aluminum (Al-7075) materials.

2. Methodology

2.1 Single Step High Pressure Torsion (SIHPT) Technique

SIHPT exposes the material to high torsional stresses under high hydrostatic pressure. Normally, the magnitude of the applied pressure is several times of the material yield strength during the last stage of SIHPT. Figure 1 illustrates a schematic of the SIHPT method for preparing a NS rod sample. As it is clear from Fig. 1, the main body of the SIHPT die consists of two casings and several steppers. This mechanism has been used for nano-structuring of metallic materials and details of this technique could be found in reference (Ref 21).

2.2 Sample Production

In the conducted experimental tests, a commercial aluminum alloy Al-7075 (composition of 0.2% Cr, 6.0% Zn, 2.8% Mg, and 1.2% Cu) and a commercially available pure copper stock with an approximate purity of 99.9% were used to prepare test samples. All samples were annealed at 700 °C for an hour before doing the SIHPT procedure. The diameter and length of the rod-shaped samples were 10 and 30 mm, respectively. A 100 Ton capacity hydraulic press was used in order to apply 5 GPa hydrostatic pressure on samples during the process. Figure 2 indicates the experimental facility used to conduct the SIHPT method for the samples processing in the current work. Each part of the sample was twisted through 5 revolutions. The equivalent strain varies between zeros at the center to approximately 22 at the outside diameter of samples (Eq 3):

$$\varepsilon_{eq} = \frac{2\pi Nr}{h\sqrt{3}} \qquad (Eq\ 3)$$

where ε_{eq} is the equivalent strain, N, r and h denote the number of SIHPT revolutions, the specimen radius and the thickness of steppers, respectively.

2.3 Microstructure Characterization

To assure that NS samples were obtained, the SIHPT processed samples were prepared for microstructural investigations under a TEM by first extracting nanoscale lamellae from the samples using a focused ion beam (FIB) method. The nanoscale lamellae were sectioned from the cross section near the edge of the sample, as shown in the schematic in Fig. 3. The thin lamellae with dimensions of $20 \times 8\ \mu m$ were prepared from the processed specimen using the *in-situ* lift-out procedure on a dual beam system (FEI NovaNanolab 600). The lamella was prepared with a thickness less than 150 nm for the following TEM characterization. Figure 4 represents the process of preparing lamella by milling process in micro level.

In addition, a field emission gun scanning electron microscope (JEOL 7100F FEGSEM) equipped with an EBSD camera (EDAX TSL) was operated at 20 kV and ~ 26 nA is used for EBSD data collection. Data was collected and then analyzed using TSL OIM Data Collection and Analysis software.

2.4 Microhardness

To evaluate changes in the hardness of the processed samples, a microhardness evaluation was used. The measurements were performed at different cross sections of the samples in axial and radial directions using a Vickers diamond indenter with an applied load of 50 gf and a dwell time of 15 s. The minimum distance between two adjacent indentations and an indentation from the edge of samples was at least 2.5 times the indentation size based on ASTM E384. This avoided any possible interactions between the work-hardened regions and edge effects. In this regard, two samples were tested that a section was taken from an 'as-drawn' rod (henceforth referred to
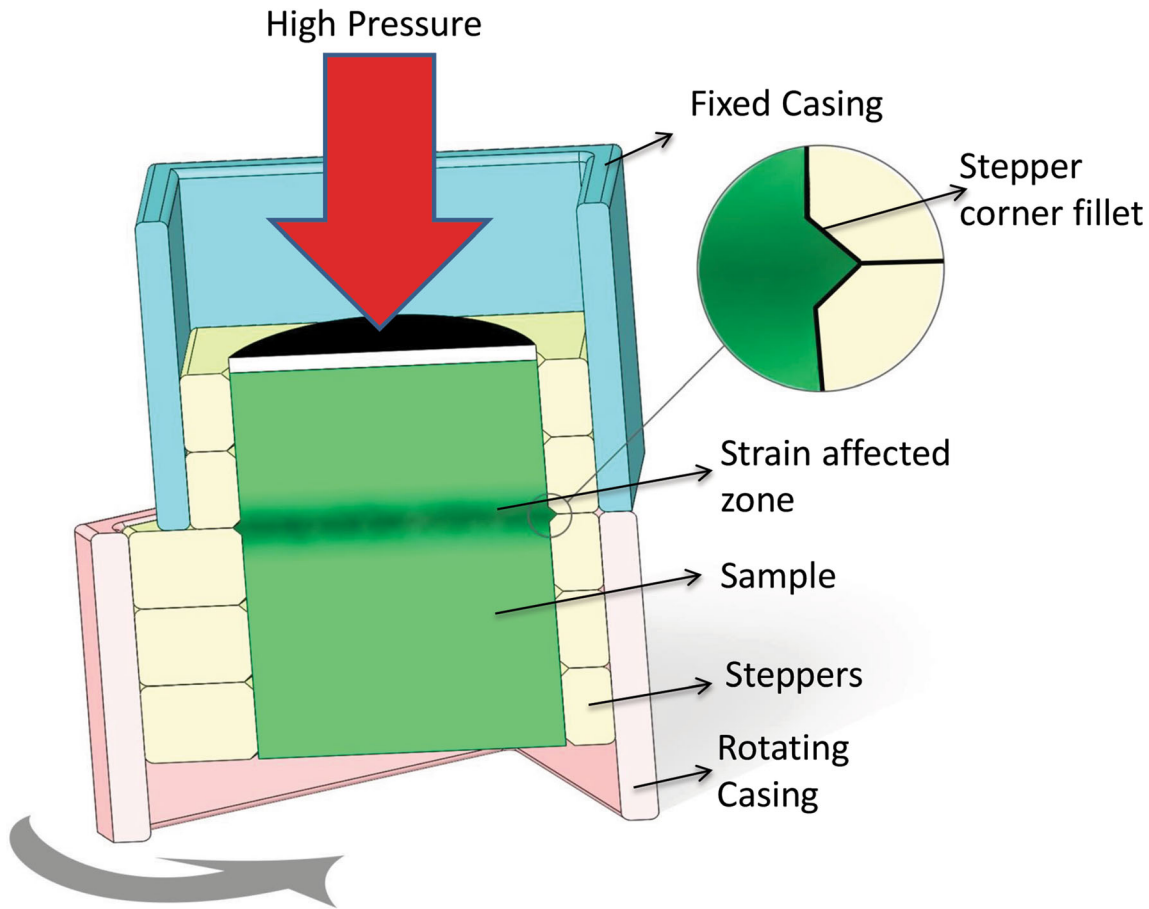
Fig. 1 Illustration of the SIHPT method

as the unprocessed sample), and a section was taken from the same designation of processed by SIHPT (henceforth referred to as the processed sample). Both samples were set in Bakelite using a Struers LaboPress-1 for ease of handling. The mounted samples were grinded by hand using progressively finer silicon carbide papers from 240 grit down to 4000 grits on a Buehler HandiMet 2.

2.5 Sample Preparation for Topographical Measurements

The surfaces of unprocessed and processed samples were prepared via grinding and polishing. The same method was applied to both sets of samples (processed and unprocessed) prior to testing and the resulting topographies were measured using white light interferometry (Alicona with the vertical measurement sensitivity of 1 nm and horizontal lateral sensitivity of 0.174 μm). Grinding of samples was performed using 240 grit, followed by 320 grit Silicon Carbide pads to ensure surface flatness. Polishing was then carried out using a Metaserv universal polisher, first with a 6 μm pad, followed by a 1 μm pad with monocrystalline diamond used as the lubricant. The samples were then rinsed under a tap and placed in an ultrasonic bath to erase the residue lubricant. These steps were repeated until the desired surface topography was achieved. White light interferometer Alicona Infinite Focus microscope with an objective magnification of $\times$ 20 was applied to measure the surface roughness parameters; Root-mean-square roughness (Rq) and root-mean-square roughness of the scanned area (Sq) of samples.

2.6 Lateral Force Microscopy (LFM)

A Dimension™ 3100 Atomic Force Microscope, made by Digital Instruments was used in the lateral mode (LFM) to measure the coefficient of boundary friction (Ref 33). A schematic of LFM system is shown in Fig. 5. As is shown in the figure, measurement is conducted using a cantilever. Due to the lateral movement of AFM, cantilever deforms and reflects the laser beam to the photodiode surface as a receiver. This reading specifies the level of deformation in cantilever which is indeed measure of friction at the interface.

A calibration procedure is required for the tip of the cantilever beam before LFM takes place for friction measurements (Ref 34, 35). Table 1 shows the specification of the AFM tip used in this study. A Bruker DNP-10 probe can be used with 4 tips, each on a separate cantilever; however, only tip A was used with a spring constant of 0.350 Nm^{-1} and a tip radius of 20 nm. Table 2 presents the set up parameters for the AFM in this analysis. Both the processed and unprocessed copper and aluminum samples were measured under nominally dry contact conditions in a controlled environment maintained at 20 °C and humidity of 45% RH with a predefined range of applied loads. It should be noted that the machine elements work at higher temperatures, but the current research is the first step towards introducing this new process. Therefore, testing at realistic temperatures and in a contact level tribometer is the next step for the further development of this proposed method.
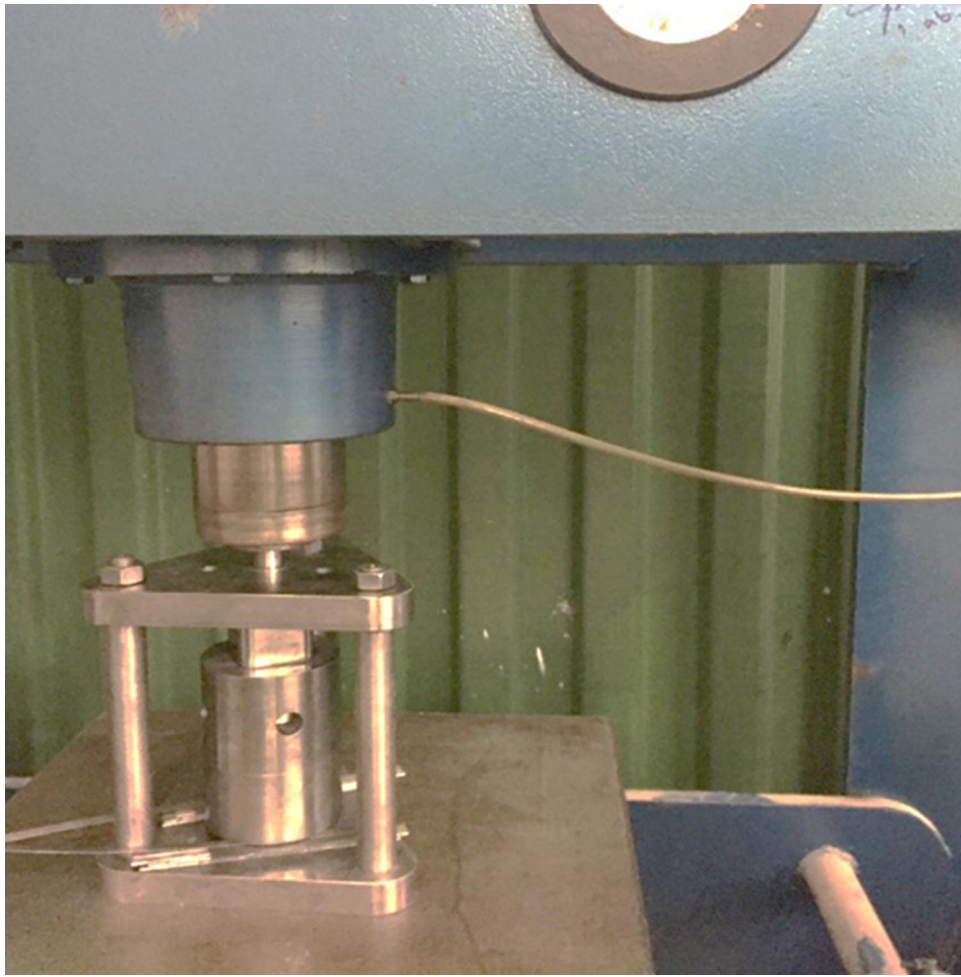
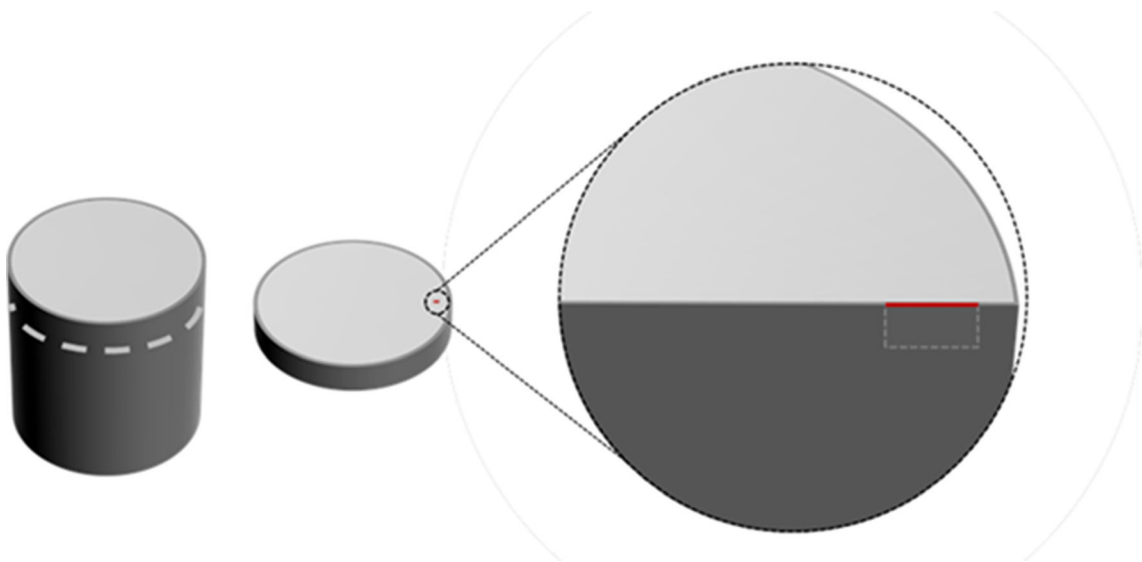**Fig. 2** SIHPT facility attached to hydraulic machine

Fig. 3 Schematic representation of the location and orientation of the nanoscale lamella extracted from the processed sample
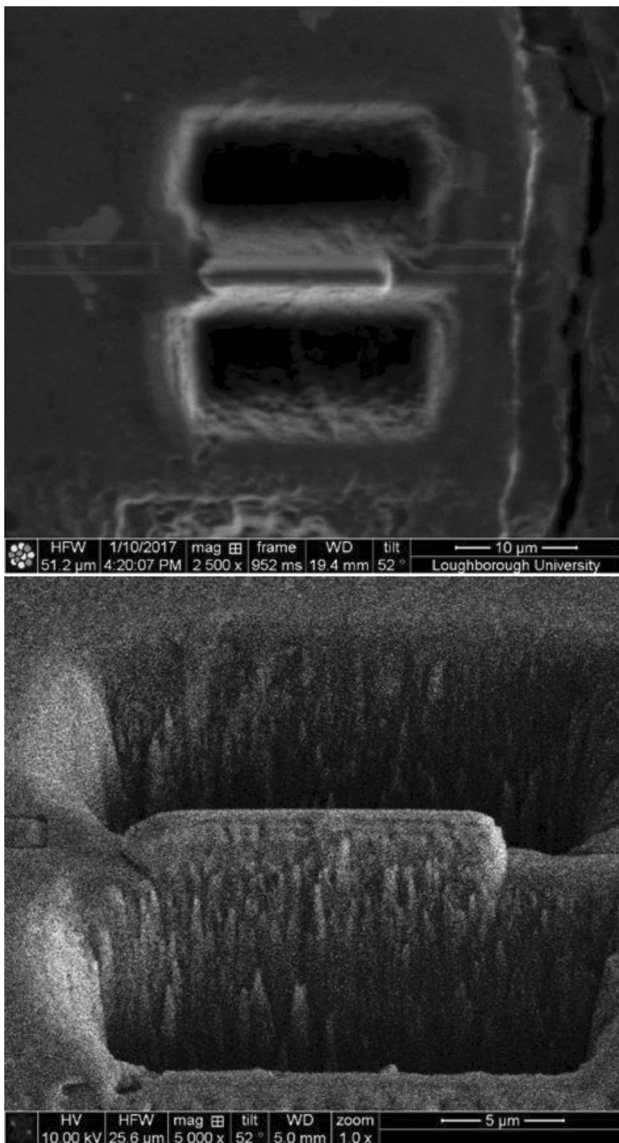
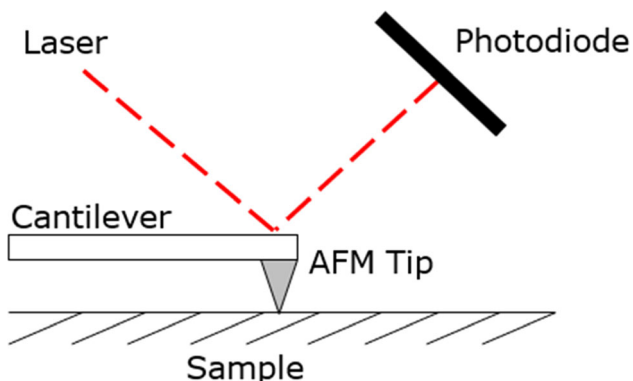**Fig. 4** An electron micrograph taken part-way through the FIB milling process

Fig. 5 Schematic of the AFM experiment

Table 1 AFM probe specification

Model	DNP-10
Material	Non-Conductive Silicon Nitride
f_0	50-80 kHz
K	0.350 Nm^{-1}
Tip radius	20 nm

Table 2 AFM set up in LFM

Parameter	Value
Scan size	1 μm
Scan rate	2 Hz
Sample lines	256
Aspect ratio	1
Integral gain	2 V
Proportional gain	3 V
Deflection set point	0 V
Scan angle (Friction)	90°

3. Results and Discussion

3.1 Microstructure Characterization Results

Electron Backscatter Diffraction (EBSD) micrographs in Fig. 6 indicate the microstructural grains of the unprocessed copper samples. The average grain sizes of both processed and unprocessed samples were found by the linear intercept method (Ref 36). As it is obvious from Fig. 6 the average grain size of unprocessed copper samples was 50 μm. TEM micrographs of the processed copper are presented in Fig. 7 which indicates that after processing a fully NS sample with an average grain size in the range of 150 nm was achieved. This corresponds to a grain size reduction of 300 times from that of the pure unprocessed copper sample.

According to Fig. 8 aluminum samples were also showed a nanostructure after processing. In the case of aluminum samples, the average grain size of the unprocessed sample was found to be ~ 550 nm while the average grain size of the processed sample was found to be ~ 150 nm.

Visual screening of TEM images in Fig. 7 and 8, reveals that the grains were not homogeneous dimensionally and the microstructures were composed of both fine and coarse grains. This combined microstructure promotes the exceptional mechanical properties for the SPD processed samples. The crucial state of the coarse and fine grain mixture at the microstructure of metals is known as bimodal grain size distribution. The effect of bimodal microstructures in NS materials is a topic that has been studied before in the literature (Ref 37).

3.2 Microhardness Results

For both copper and aluminum samples, the processed samples had a greater hardness than that of the unprocessed samples at every point measured along the samples' radii as detailed in Fig. 9. This is due to the fact that the hardness of the cold worked material increases with increase in the dislocation
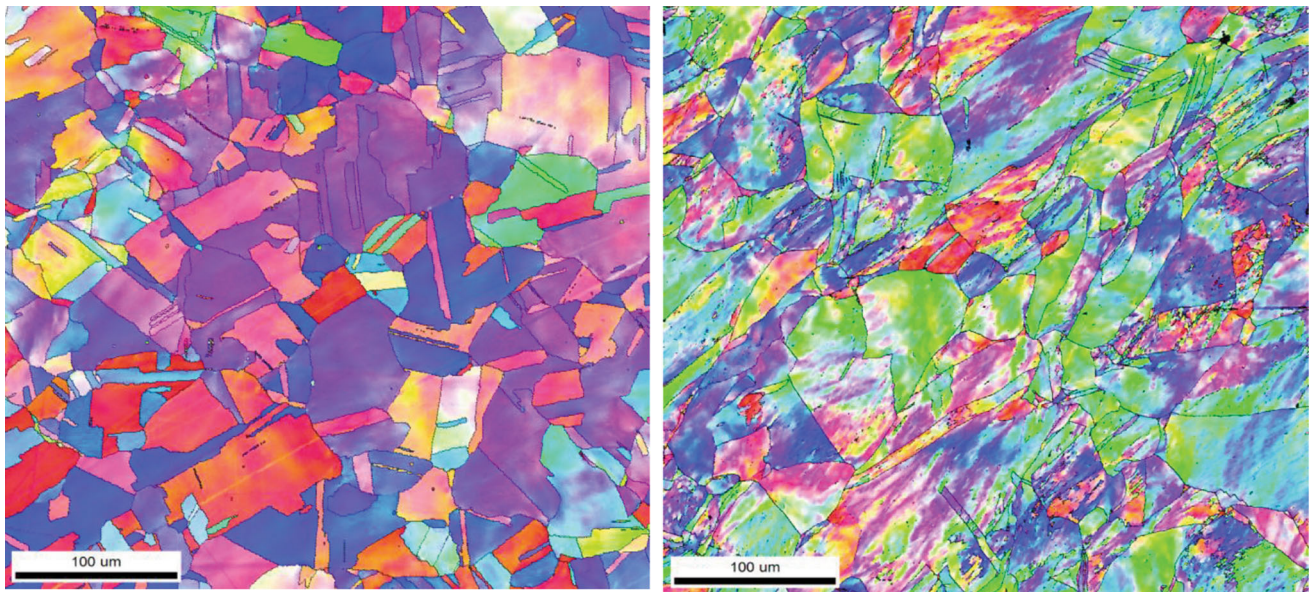
Fig. 6 EBSD graph of the original and annealed copper sample which shows the grain sizes were in orders of several micrometers
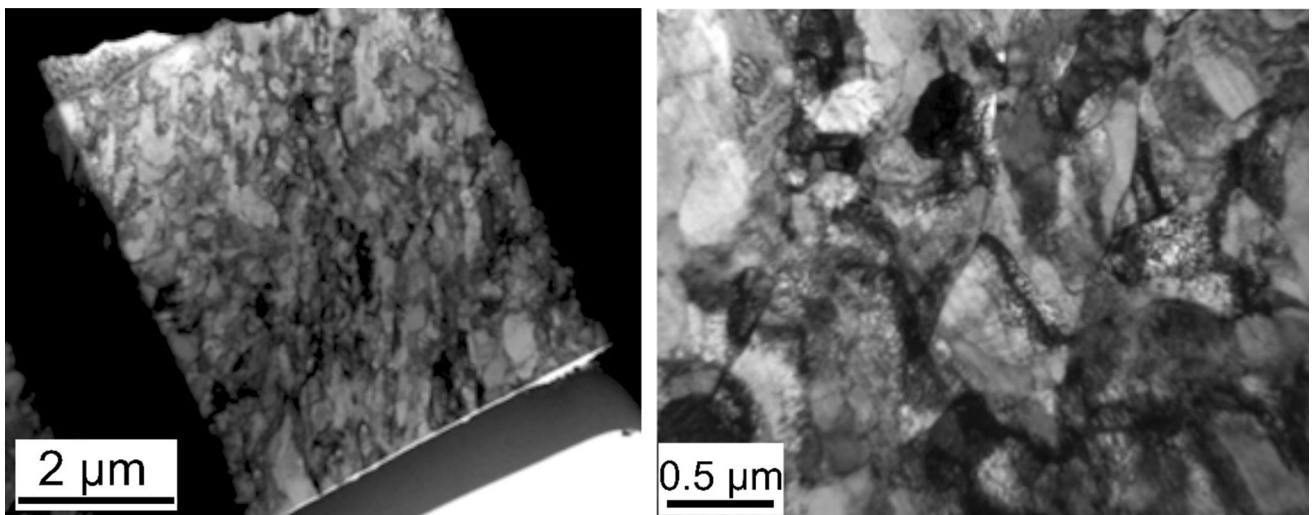

Fig. 7 TEM micrograph of a SIHPT processed copper sample which shows fully nanostructured grain sizes

density. The rate of strains and cold work in SIHPT is more in outer radii; therefore, outer radii of the sample show higher hardness than the inner sections and accordingly, the results of Fig. 9 is reasonable. The increased hardness after undergoing nano-structuring was expected to alter the friction generated in the adhesion-dominated regime.

3.3 Topographical Measurements

Figure 10 and 11 present the surface topography of copper and aluminum samples. Using these plots, the surface roughness parameters could be obtained, as listed in Table 3. The processed sample was further polished to check the roughness independency of the AFM results, as explained later. Considering the measured grain sizes and the surface roughness values

in Table 3, indicates that the ratio of asperities height-to-grain size in unprocessed, processed and highly polished surface of the processed samples were 0.016, 3.73 and 0.025, respectively.

3.4 Lateral Force Microscopy (LFM)

The taken measurements using the AFM were from the edge of each sample, where the greatest degree of plastic deformation took place for the processed sample. For the anticipated application of this paper, which is the rolling element for automotive bearings, the edge of the samples has been the most appropriate locations since the conjunction between the rolling element and the bearing races take place at the outer diameter. The measurements were taken as an average of 3 points selected circumferentially with equal spacing of 120 degrees.

The averages summarized in Fig. 12 for (12a) aluminum and (12b) copper samples, respectively, where the gradient was representative of the boundary shear strength of asperities, ζ, which corresponds to the COF of the asperities. The average standard deviation for data of processed and unprocessed aluminum samples were 1.4 and 1.2 nN, respectively. In Fig. 12 the processed samples have the lowest coefficient of boundary friction, when compared to the unprocessed samples. This is representative of a 45 and 25% reduction in the COF for aluminum and copper samples, respectively, whereby the presented results were for single scans of each sample, measuring 256×256 data points over an area of $1 \mu m^2$.
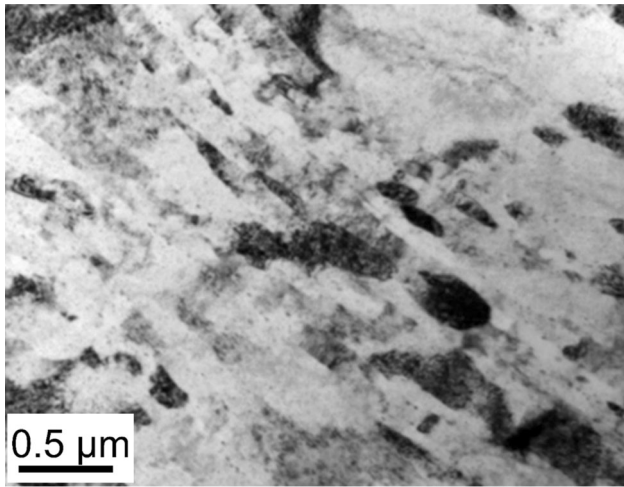
The reduction in friction could be explained by the balance between adhesive and ploughing components of friction. The increased hardness of the processed samples increases ploughing friction in accord with Eq 2. Conversely, higher hardness reduces the real area of contact, thus diminish adhesive friction. For the presented samples, these competing contributions favor a reduction in adhesive friction rather than an enhancement in ploughing friction. In another word, the COF depends on the ration of the asperities tip radii to grain size of the material microstructure (Ref 29). When the average grain size is smaller than the tip sizes, the COF is inversely proportional to hardness. The NS materials have higher hardness and therefore, the reduced COF is expected.

4. Conclusion

Nanostructured Al-7075 and pure copper samples applying SPD method were obtained through the current study. Tribological performance of the processed and unprocessed samples were compared. Measurements based on TEM micrographs indicated that the NS samples had the average grain size of ~ 150 nm. The micrographs' observations revealed that the microstructures were composed of fine and coarse grain sizes. In addition, according to Vickers microhardness measurements, the hardness of the processed samples showed substantial increases. The changes in hardness and the microstructural patterns were reflected in the friction coefficient reduction of aluminum and copper samples by 45 and 25%, respectively. The reduction in the friction could be explained by the balance between adhesive and ploughing components of the friction. The increased hardness of the processed samples augment the ploughing friction in accord with Eq 2. Conversely, higher hardness decline the real area of contacts, thus reduces the
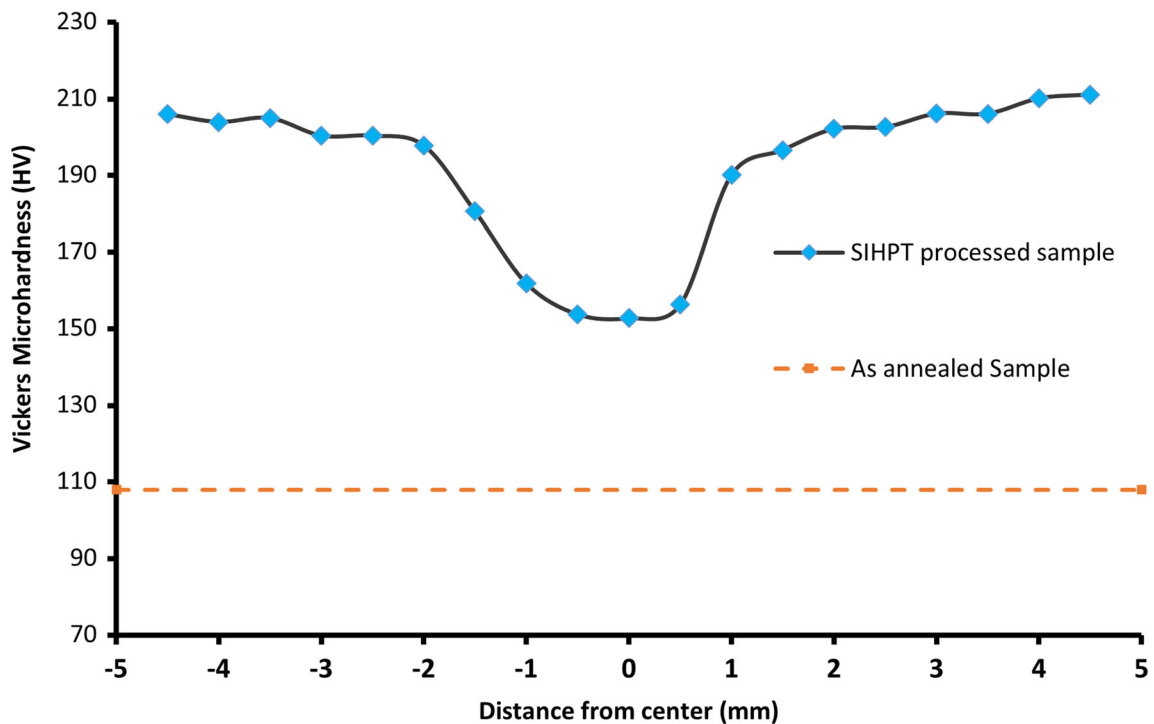

Fig. 8 A bright field TEM micrograph of the microstructure of the processed aluminum sample

Fig. 9 Comparison of microhardness measurements in as annealed and SIHPT processed aluminum samples
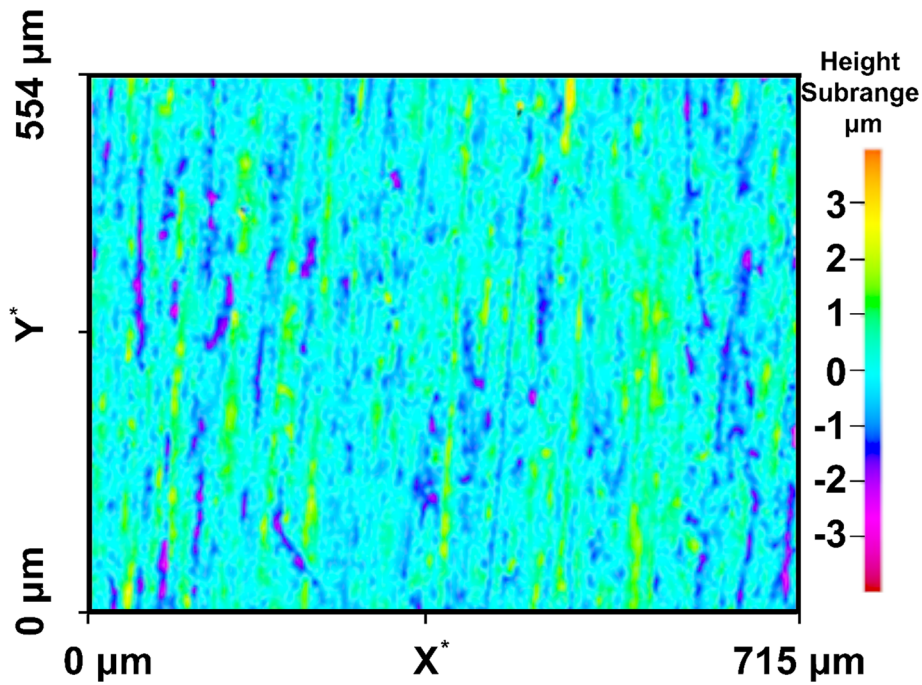
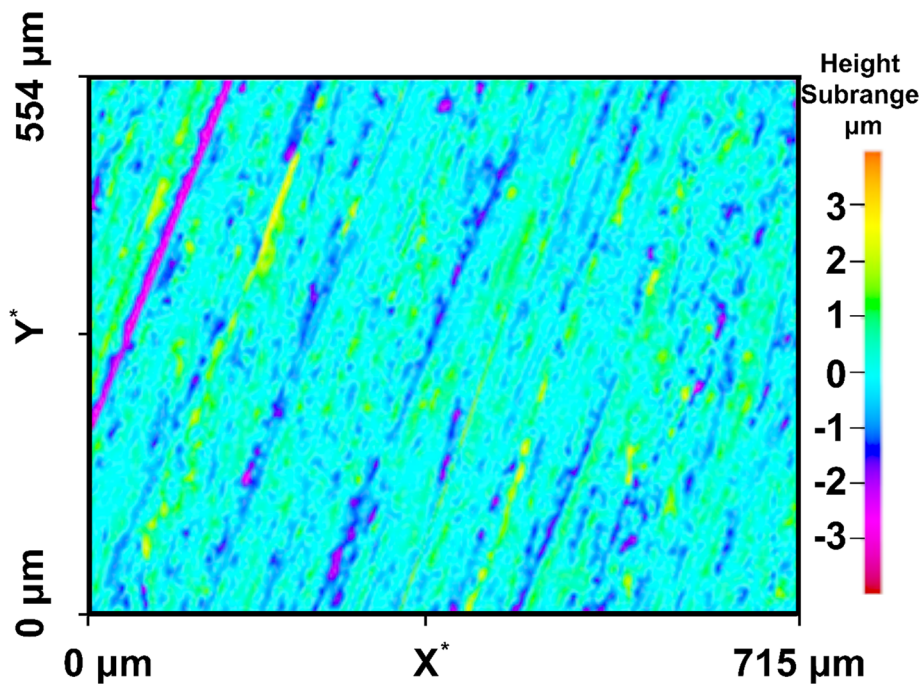**Fig. 10** Surface topography of the unprocessed copper sample

Fig. 11 Surface topography of the processed copper sample

Table 3 Surface topographical measures for aluminum samples

Sample	Rq, nm	Sq, nm
Unprocessed	620.09	657.13
Processed	559.20	649.33
Processed (Highly polished)	3.75	6.83

adhesive friction. For the presented samples, these competing contributions favor a reduction in the adhesive friction rather than an enhancement in the ploughing friction. Obtained superior frictional characteristics of copper and aluminum as well as surface hardness of lightweight aluminum alloy proposes ideal combination of the material and process for the rolling element of automotive bearings specially at ultra-high speeds. Further study is required to assess the performance of these processed materials at contact, component and system level for a rolling element bearing. These assessments can be
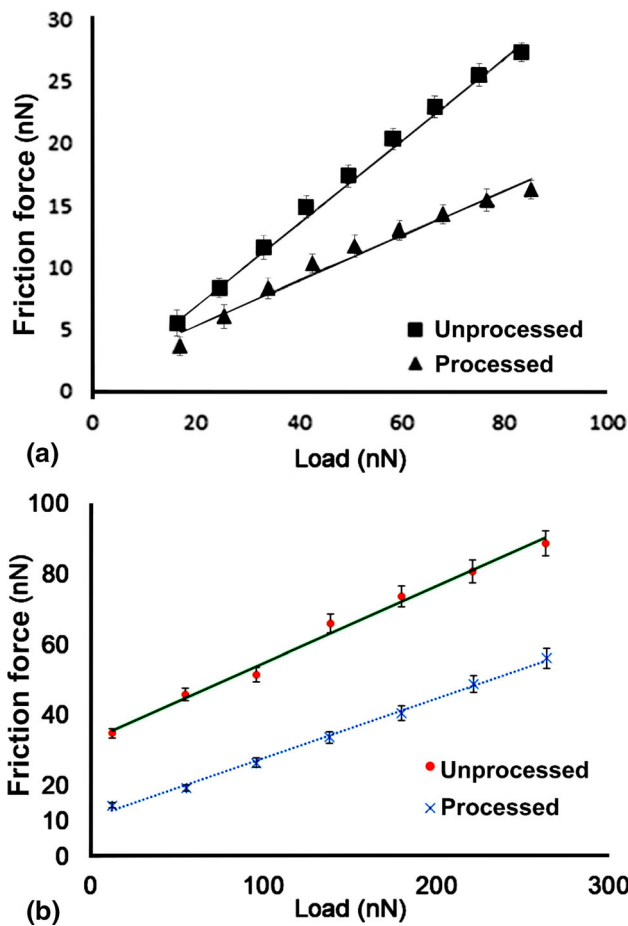
Fig. 12 LFM measured friction versus load for (a) aluminum, and (b) copper samples under nominally dry conditions

performed in contact level tribometers or component/system level test rigs.

Conflict of Interest

There is not any conflict of interest concerning the stages of data collection and analysis, interpretation of results and writing during the preparation of the manuscript.

Open Access

References

1. H. Questa, M. Mohammadpour, S. Theodossiades, C.P. Garner, S.R. Bewsher, and G. Offner, Tribo-dynamic Analysis of High-Speed Roller Bearings for Electrified Vehicle Powertrains, *Tribol. Int.*, 2021, **154**, 106675
2. R.Z. Valiev, Y. Estrin, Z. Horita, T.G. Langdon, M.J. Zechetbauer, and Y.T. Zhu, Producing Bulk Ultrafine-Grained Materials by Severe Plastic Deformation, *JOM*, 2006, **58**(4), p 33–39
3. B. Leszczyńska-Madej, P. Pałka, and M. Richert, Effect of Severe Plastic Deformation on Microstructure and Properties of Polycrystalline Aluminium Al99. 5, *Archives of Metallurgy and Materials*, **59**, (2014)
4. A. Shahsavari, F. Karimzadeh, A. Rezaeian, and H. Heydari, Significant Increase in Tensile Strength and Hardness in 2024 Aluminum Alloy by Cryogenic Rolling, *Procedia Mater. Sci.*, 2015, **11**, p 84–88
5. C. Choi and N. Roberts, Simple Model for Effective Thermal Conductivity of Bulk Nanostructured Materials, *Int. J. Therm. Sci.*, 2016, **104**, p 13–19
6. P. Allia, P. Tiberto, M. Baricco, M. Knobel, and F. Vinai, Nanostructured Materials for Soft Magnetic Applications Produced by Fast DC Joule Heating, *IEEE Trans. Magn.*, 1994, **30**(6), p 4797–4799
7. A.S. Aricò, P. Bruce, B. Scrosati, J.-M. Tarascon, and W. van Schalkwijk, Nanostructured Materials for Advanced Energy Conversion and Storage Devices, *Nat. Mater.*, 2005, **4**(5), p 366–377
8. A. El-Meligi, Nanostructure of Materials and Corrosion Resistance, *Dev. Corros. Prot.* 3–23 (2014)
9. R.Z. Valiev and I.P. Semenova, Advances in Superplasticity of Ultrafine-Grained Alloys: Recent Research and Development, *Mater. Sci. Forum*, 2016, **838-839**, p 23–33
10. R. Gohar, H. Rahnejat, Bio-tribology (skin) Fundamentals of Tribology, ed., London: World Scientific Publishing Co, 2012
11. F. Marra, L. Baiamonte, C. Bartuli, M. Valente, T. Valente, and G. Pulci, Tribological Behaviour of Alumina-Titania Nanostructured Coatings Produced by Air Plasma Spray Technique, *Chem. Eng. Trans.*, 2016, **47**, p 127–132
12. T. Masalehdan, M. Eskandarzade, A. Tutunchi, B. Kim, H. Questa, M. Mohammadpour, and M. Shahedi Asl, Two-Dimensional Clay Nanosheet-Reinforced Polytetrafluoroethylene Composites and Their Mechanical/Tribological Studies, *Mater. Today Commun.*, 2021, **26**, p 102026
13. G. Di Girolamo, F. Marra, L. Pilloni, G. Pulci, J. Tirillò, and T. Valente, Microstructure and Wear Behavior of Plasma-Sprayed Nanostructured WC-Co Coatings, *Int. J. Appl. Ceram. Technol.*, 2013, **10**(1), p 60–71
14. L. Baiamonte, F. Marra, G. Pulci, J. Tirillò, F. Sarasini, C. Bartuli, and T. Valente, High Temperature Mechanical Characterization of Plasma-Sprayed Zirconia-Yttria from Conventional and Nanostructured Powders, *Surf. Coat. Technol.*, 2015, **277**, p 289–298
15. S.V. Prasad, C.C. Battaile, and P.G. Kotula, Friction Transitions in Nanocrystalline Nickel, *Scr. Mater.*, 2011, **64**(8), p 729–732
16. H.A. Padilla, B.L. Boyce, C.C. Battaile, and S.V. Prasad, Frictional Performance and Near-Surface Evolution of Nanocrystalline Ni-Fe as Governed by Contact Stress and Sliding Velocity, *Wear*, 2013, **297**(1), p 860–871
17. N. Gao, C.T. Wang, R.J.K. Wood, and T.G. Langdon, Tribological Properties of Ultrafine-Grained Materials Processed by Severe Plastic Deformation, *J. Mater. Sci.*, 2012, **47**(12), p 4779–4797
18. K. Tonotsuka, Y. Todaka, N. Adachi, K. Horii, M. Toda, M. Mitsuhara, M. Iwasaki, Y. Shiihara, Y. Umeno, and M. Nishida, Effect of Lattice Defects on Tribological Behavior for High Friction Coefficient under TCP Added PAO Lubrication in Nanostructured Steels, *ISIJ Int.*, ISIJINT-2019–2707 (2020)
19. G.K. Manjunath, G.V. Preetham Kumar, and K. Udaya Bhat, Evolution of Tribological Properties of Cast Al-10Zn-2Mg Alloy Subjected to Severe Plastic Deformation, Structural Integrity Assessment, R.V. Prakash, R. Suresh Kumar, A. Nagesha, G. Sasikala, A.K. Bhaduri Eds., 2020//, 2020 (Singapore), Springer Singapore, pp 165–175
20. L. Su, G. Deng, and A.K. Tieu, Effect of Severe Plastic Deformation on Mechanical and Tribological Properties of Aluminium Alloys, International Conference on Nanostructured Materials (NANO 2020), 2020, Engineers Australia Melbourne, p 99
21. M. Eskandarzade, A. Masoumi, G. Faraji, M. Mohammadpour, and X.S. Yan, A New Designed Incremental High Pressure Torsion Process

for Producing Long Nanostructured Rod Samples, *J. Alloys Compd.*, 2017, **695**, p 1539–1546

22. B. Bharat, Handbook of Micro/Nano Tribology, *Bharat.-1999*, (1999)

23. L. Lu, X. Chen, X. Huang, and K. Lu, Revealing the Maximum Strength in Nanotwinned Copper, *Science*, 2009, **323**(5914), p 607–610

24. A.S. Miavaghi, H. Kangarlou, and M. Eskandarzade, Comparison Between Frictional Behavior of the Soft and Brittle Materials at Different Contact Pressures, *Leban. Sci. J.*, 2017, **18**(1), p 98–105

25. A.K. Dzhanakhmedov, Tribological Phenomena during Contact Interactions in Nanostructured Coatings, *J. Frict. Wear*, 2020, **41**(1), p 46–51

26. Z.N. Farhat, Y. Ding, D.O. Northwood, and A.T. Alpas, Effect of Grain Size on Friction and Wear of Nanocrystalline Aluminum, *Mater. Sci. Eng. A*, 1996, **206**(2), p 302–313

27. L.F. Peng, M.Y. Mao, M.W. Fu, and X.M. Lai, Effect of Grain Size on the Adhesive and Ploughing Friction Behaviours of Polycrystalline Metals In Forming Process, *Int. J. Mech. Sci.*, 2016, **117**, p 197–209

28. N. Beckmann, P.A. Romero, D. Linsler, M. Dienwiebel, U. Stolz, M. Moseler, and P. Gumbsch, Origins of Folding Instabilities on Polycrystalline Metal Surfaces, *Phys. Rev. Appl.*, 2014, **2**(6), 064004

29. A. Li and I. Szlufarska, How Grain Size Controls Friction and Wear in Nanocrystalline Metals, *Phys. Rev. B*, 2015, **92**(7), 075418

30. M. Zha, H.-M. Zhang, Yu. Zhi-Yuan, X.-H. Zhang, X.-T. Meng, H.-Y. Wang, and Q.-C. Jiang, Bimodal Microstructure—A Feasible Strategy for High-Strength and Ductile Metallic Materials, *J. Mater. Sci. Technol.*, 2018, **34**(2), p 257–264

31. S.G. Kumbhar, P.E. Sudhagar, and R.G. Desavale, An Overview of Dynamic Modeling of Rolling-Element Bearings, *Noise Vib. Worldwide*, 2021, **52**(1-2), p 3–18

32. Z. Liu, C. Song, J. Li, X. Hou, Li. Wang, and Y. Zhang, Effect of Rotation Speed on Electric Damage of Copper Tribo/Electric Rolling Pairs under Lubricated Single-Point Contact, *Mater. Trans.*, 2020, **61**(1), p 111–118

33. W.W.F. Chong and H. Rahnejat, Nanoscale Friction as a Function of Activation Energies, *Surf. Topogr. Metrol. Prop.*, 2015, **3**(4), 044002

34. C.K. Buenviaje, S.R. Ge, M.H. Rafailovich, and R.M. Overney, Atomic Force Microscopy Calibration Methods for Lateral Force, Elasticity, and Viscosity, *MRS Proc.*, 1998, **522**, p 187

35. G. Styles, R. Rahmani, H. Rahnejat, and B. Fitzsimons, In-Cycle and Life-Time Friction Transience in Piston Ring-Liner Conjunction under Mixed Regime of Lubrication, *Int. J. Engine Res.*, 2014, **15**(7), p 862–876

36. E. Santecchia, P. Mengucci, and M. Cabibbo, Microstructure and Intermetallic Strengthening in an Equal Channel Angular Pressed AA2219. Part I: Microstructure Characterization, *Metallogr. Microstruct. Anal.*, 2014, **3**(3), p 194–202

37. H.W. Höppel, M. Korn, R. Lapovok, and H. Mughrabi, Bimodal Grain Size Distributions in UFG Materials Produced by SPD: Their Evolution and Effect on Mechanical Properties, *J. Phys. Conf. Ser.*, 2010, **240**, 012147

Publisher's Note Springer Nature remains neutral with regard to jurisdictional claims in published maps and institutional affiliations.